Food Chemistry: X 27 (2025) 102456

Contents lists available at ScienceDirect

Food Chemistry: X

journal homepage: www.sciencedirect.com/journal/food-chemistry-x

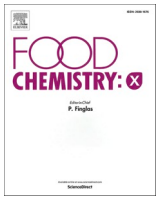

Composite solutions of Phycocyanin and chitosan extend oyster shelf life

Yan Li [a,b,1], Li Liu [a,b,1], Youwei Du [a,b], Zihao Yin [c], Yue Zhao [a,b], Guangxin Feng [a,b], Mingyong Zeng [a,b,*]

[a] College of Food Science and Engineering, Ocean University of China, Qingdao 266003, China
[b] State Key Laboratory of Marine Food Processing & Safety Control, Shandong Province Engineering Research Centre of Marine Food Preservation and Quality Control, China
[c] College of Biosystems Engineering and Food Science, Zhejiang University, Hangzhou 310058, China

ARTICLE INFO

Keywords:
Chitosan
Phycocyanin
Composite solution
Antioxidant activity
Antimicrobial property
Oyster preservation

ABSTRACT

Phycocyanin (PC), a blue antioxidant and anti-inflammatory pigment, was combined with 2.5 % chitosan (CTS) to form stable composite solutions. This study aimed to develop a CTS-PC composite solution with enhanced antioxidant and antimicrobial properties to improve oyster preservation. Structural compatibility was confirmed through scanning electron microscopy and X-ray diffraction. Viscosity and contact angle analyses demonstrated encapsulation and barrier properties. Fourier-transform infrared spectroscopy, circular dichroism, zeta potential, and particle size analyses revealed that hydrogen bonding, hydrophobic interactions, and electrostatic forces contributed to stability. PC enhanced hydrophobicity and antioxidant capacity, and the 0.05 % PC/CTS solution exhibited the best strongest inhibition against *Pseudomonas aeruginosa* (19.14 ± 0.08 mm). Immersion extended oyster shelf life from 4 days (control) to 12 days (0.1 % PC/CTS), outperforming the commercial preservative (6 days). These findings highlight the potential of this safe, eco-friendly preservation strategy for oysters and other chilled aquatic products.

1. Introduction

Aquaculture has grown steadily in recent decades, with shellfish and algae accounting for nearly half of total production. The Rushan oyster, valued for its high protein and polyunsaturated fatty acid content, dominates China's premium oyster market. Shucked oysters offer convenience but are prone to oxidation and quality deterioration due to increased exposure and mechanical damage. Previous studies have demonstrated that n-3 PUFA can induce oxidative stress through ROS generation (Liu et al., 2020). This suggests that seafood rich in n-3 PUFA is prone to oxidation during storage, leading to quality deterioration. Traditional oyster preservation methods, such as freezing, canning, dry storage, and air conditioning (Cao, Xue, & Liu, 2009), are unsuitable for commercial applications owing to the high equipment and transportation costs. Therefore, there is an urgent need to develop a green and efficient method for oyster preservation.

Chand et al. (Chand, 2024) analyzed 49 studies from 2000 to 2023 on nontraditional fish preservation and found chemical methods most effective. However, preservatives like nitrates and potassium sorbate, though effective against spoilage bacteria in oysters, pose health risks such as cytotoxicity and oxidative stress. Natural preservatives are expected to replace synthetic ones due to safety concerns. In recent years, natural extracts have gained attention for their safety, eco-friendliness, and antibacterial/antioxidant properties. Currently, most natural substances are applied through short-term immersion or surface coating (Cao, Xue, & Liu, 2009; Costa, Conte, & Del Nobile, 2014; Zhao et al., 2024). Although these methods demonstrate noticeable short-term effects, their effectiveness often declines with prolonged storage. The solution immersion preservation method addresses this limitation by immersing food in solutions enriched with specific functional ingredients for prolonged periods, significantly enhancing long-term preservation.

Phycocyanin (PC) is a blue photosynthetic pigment protein primarily found in cyanobacteria such as spirulina; it accounts for 20 % of the total protein content of spirulina (Golmakani, Hajjari, Kiani, Sharif, & Hosseini, 2024). Its bright and distinctive color, natural origin, and excellent light-harvesting properties make PC a promising candidate for use in functional foods and cosmetics. PC is the primary source driving

* Corresponding author.
E-mail address: mingyz@ouc.edu.cn (M. Zeng).
[1] These authors contributed equally to this work.

https://doi.org/10.1016/j.fochx.2025.102456
Received 5 March 2025; Received in revised form 7 April 2025; Accepted 9 April 2025
Available online 15 April 2025

spirulina's commercial value, with projections indicating that the global PC market could surpass $400 million by 2030 (Chini Zittelli, Lauceri, Faraloni, Silva Benavides and Torzillo, 2023). The active groups in PC, including tryptophan, tyrosine, and other amino acid residues, contribute to its effective reducing and antioxidant properties. Phycocyanobilin (PCB), a linear tetrapyrrole compound, stabilizes free radicals and inhibits free radical chain reactions, providing it with significant free radical scavenging capabilities. These structures and functions confer PC with various biological properties. The antioxidant, anticancer, antibacterial, immunomodulatory, and anti-inflammatory activities of PC have been demonstrated through in vitro and in vivo experiments (Chen et al., 2024; Bergandi, Apprato, & Silvagno, 2022; Guo et al., 2020; Omar et al., 2022; Rathnasamy, Rajendran, Balaraman, & Viswanathan, 2019). Tavakoli et al. (Tavakoli et al., 2023) developed a grass carp freshness indicator card by blending anthocyanin, PC, and gelatin, utilizing natural pigments that exhibit different colors under varying pH conditions. Additionally, studies have demonstrated that carbohydrates inhibit protein aggregation through electrostatic binding interactions with protein surfaces and hydration, thereby improving protein stability under acidic and high-temperature conditions (Li, Zhang and Abbaspourrad, 2021). While previous studies, such as Li et al. (Li et al., 2023), have demonstrated the ability of carboxymethyl chitosan (CTS) to stabilize phycocyanin (PC) for its colorant applications, the combination of CTS and PC has not been extensively explored for food preservation. Our study extends the potential of the PC/CTS composite by focusing on its antibacterial properties, shelf-life extension, and overall preservation of oysters, a novel application not addressed by previous studies.

CTS is derived from the natural polysaccharide chitin, which is found in the exoskeleton of crustaceans and arthropods. CTS possesses various biological activities, including bacteriostatic, biodegradable, antioxidant, and anti-inflammatory properties, and is widely utilized in the food, cosmetics, and textile industries (Ul-Islam et al., 2024; Yan, Zhang, Lai, Wang, & Wu, 2024). In food preservation, CTS can be used as an edible coating applied directly to food surfaces owing to its excellent preservation and film-forming properties, offering promising application prospects (Shaikh, Yaqoob, & Aggarwal, 2021). CTS-based films with ε-polylysine and catechuic acid have been used to preserve chilled pork (Zhang, Han, & Zhou, 2024). CTS infused with lemongrass oil has extended salmon refrigeration (Yin et al., 2022), and a smart indicator card made of CTS and gelatin with pea anthocyanins monitors beef freshness (Li, Li, & Abbaspourrad, 2024). Due to its low antioxidant activity, CTS is often combined with natural antioxidants like polyphenols and essential oils (Liu, Liao, & Xia, 2023).

This study aimed to develop a green preservative to extend the refrigerated shelf life of oysters by creating a composite of PC and CTS. The physicochemical properties and bioactivities (antioxidant and antimicrobial) of the composite its effect on the refrigerated preservation of shucked oysters were systematically evaluated. The innovative use of phycocyanin (PC) in combination with chitosan (CTS) through a prolonged immersion method provides a sustainable and efficient alternative for oyster preservation, offering a new approach compared to traditional methods and extending its potential for other aquatic products.

2. Materials and methods

2.1. Materials

Live Rushan oysters with fresh dry hay odor were purchased from a farmers' market in Qingdao, China, during the summer season. The oysters had a shell length of approximately 10–15 cm and an individual weight of 120–180 g. They were transported to the laboratory under ice bath conditions and immediately shucked upon arrival. Fresh oysters were sourced from local markets. Dried PC powder was purchased from Xindaze Biotech Co., Ltd. (Fujian, China). CTS (DS261173) was provided by Anhui Cool Bioengineering Co. (China). Citrate (10007118) was obtained from Sinopharm Chemical Reagent Co. (China).

2.2. Preparation and characterization of PC/CTS solution

2.2.1. Preparation of PC/CTS solution

PC (0.2 g/mL) was dissolved in pure water using a magnetic stirrer (SHJ-4 A, Changzhou Putian Instrument Manufacturing Co., Ltd., China) for 6 h at room temperature (25 °C). CTS (2.5 %, *w*/w) was dissolved in citric acid (3 %, *w/v*) with a magnetic stirrer at 50 °C. Air bubbles were removed using an ultrasonic cleaner (KQ-300VDE, Kunshan Ultrasonic Instrument Co., Ltd., China). The prepared PC solution was then combined with the CTS solution to form a mixture containing PC at concentrations of 0.05, 0.1, 0.2, and 0.4 %. This mixture was stirred at 40 °C for 1 h.

2.2.2. Color and transparency

A colorimeter (NR60CP, Shenzhen Sanhui Technology Co., Ltd., China) was used to measure the color of the composite solution. Before measurement, the colorimeter was calibrated using a white standard plate (L* = 92.61, a* = 0.19, b* = 4.43). For each sample, five uniformly flat locations were selected, and the total color difference (ΔE) was calculated using the following equation:

$$\Delta E = \sqrt{(\Delta L^*)^2 + (\Delta a^*)^2 + (\Delta b^*)^2} \quad (1)$$

where ΔL* represents the difference in brightness, Δa* represents the difference between red and green, and Δb* represents the difference between yellow and blue.

For the transparency test, the composite solution was dried, cut into 50 mm × 10 mm strips, and analyzed using a UV spectrophotometer (UV-2550, Shimadzu, Japan). A wavelength range of 200–800 nm was used for scanning, and the absorbance value of the composite film at 600 nm was recorded. The opacity was then calculated using the following equation:

$$O_p = \frac{Abs_{600}}{T} \quad (2)$$

where T represents the thickness of the strip.

2.2.3. pH, polydispersity index, particle size, and zeta potential of the PC/CTS solution

The pH of the composite solution was measured using a pH meter (PHS-3C, Ray Magnetics, China). Particle size, polydispersity index (PDI), and zeta potential were analyzed with a nanoparticle sizer (Nano ZS90, Malvern Instruments, UK). Samples were diluted 100-fold with ultrapure water (18.2 MΩ·cm resistivity) to optimize light scattering (count rate 200–300 kcps). Three measurements (30 runs each) were performed at 25 ± 0.1 °C. *zeta* potential was calculated from electrophoretic mobility using the Smoluchowski approximation (ε = 78.5).

2.2.4. Fourier transform infrared (FTIR) spectroscopy

An FTIR spectrometer (Nicolet iS10, Thermo Fisher Scientific, USA) was used to analyze changes in functional groups within the composite solution. To eliminate the effect of moisture, the freshly prepared composite solution was lyophilized. The spectral range of 4000–400 cm^{-1} was selected, and the samples were scanned 64 times for analysis.

2.2.5. Circular dichroism (CD) spectroscopy

The protein structure of the composite solution was analyzed using a CD spectrometer (Jasco 1500, Jasco, Japan). Measurements were conducted across a wavelength range of 190–260 nm, with a scanning speed of 100 nm/min, bandwidth of 1 nm, and data pitch of 0.5 nm.

2.2.6. Viscosity

The rheological properties of the composite solutions were analyzed using a rheometer (MCR30203052207, Anton Paar, Austria) following the method outlined by Liu et al. (Liu et al., 2022). The apparent viscosity of the solutions was measured at 25 °C across a shear rate range of 0.1–100 s^{-1}, with pure water serving as the control.

2.2.7. X-ray diffraction (XRD)

An X-ray diffractometer (Smart Lab 3KW, Rigaku, Japan) was used to analyze the XRD intensity distribution of the composite solution after drying. Cu Kα radiation was employed at 20 °C with a scanning speed of 2°/min, and the diffraction angle (2θ) was set within the range of 10°–80°.

2.2.8. Antibacterial activity evaluation

Following the method described by Zhang et al. (Zhang et al., 2023), the inhibitory effect of the composite solution on *Pseudomonas aeruginosa* (PA14, obtained from our laboratory) and total oyster spoilage bacteria (*P. aeruginosa*, isolated from spoiled oysters) was evaluated using the circlezone of inhibition method. Ten-millimeter disks were submerged in the composite solution for 5 min, dried, sterilized under UV light for 20 min, and then prepared for use. To determine the *P. aeruginosa* zone of inhibition, 0.2 mL of a bacterial suspension at a concentration of 10^6 CFU/mL was added to CFC medium and incubated at 28 °C for 48 h. For total oyster spoilage bacteria, 0.2 mL of a bacterial suspension at a concentration of 10^6 CFU/mL was added to LB medium and incubated at 28 °C for 24 h. At the end of the experiment, the inhibition zone diameter was measured using a vernier caliper with an accuracy of 0.02 mm.

2.2.9. Scanning electron microscopy (SEM)

SEM was performed to examine the surface morphology of the samples using a scanning electron microscope (JSM-5800, JEOL Ltd., Japan). The cross-sectional and surface morphology of the dried composite solution sheet were observed at a magnification of 3000× under an accelerating voltage of 20 kV. Before analysis, the samples were fixed and sputter coated with gold.

2.2.10. Contact angle

Following the method described by Li et al. (Li, Li, & Abbaspourrad, 2024), the composite solution was dried, placed, and fixed on the horizontal removable plate of a contact angle device (SDC-200S, Shengding, China). Photographs of 5 μL water droplets in contact with the sample were taken immediately after being vertically dropped onto the composite membrane, and the contact angle was measured.

2.2.11. DPPH scavenging effect

The DPPH scavenging effect of the composite solution was determined following the method described by Sun et al. (Sun, Wei, & Xue, 2023). Briefly, 50 mg of the composite solution was dissolved in 5 mL of pure water to form a sample solution, which was thoroughly mixed to ensure uniform distribution. The sample solution was then mixed with DPPH–ethanol solution (0.2 mM) in a 1:2 ratio and stored at room temperature for 30 min, protected from light. The absorbance of different samples was measured at 517 nm, and the DPPH radical scavenging rate was calculated using the following equation:

$$\text{DPPH savenging effect}(\%) = \frac{A_{DPPH} - (A_{S-DPPH} - A_b)}{A_{DPPH}} \times 100\% \quad (3)$$

A_{DPPH} represents the absorbance of the initial DPPH–ethanol solution. $A_{s\text{-}DPPH}$ refers to the absorbance at 517 nm after mixing the DPPH–ethanol solution with the sample solution. A_b indicates the absorbance measured at 517 nm after mixing the DPPH solution with anhydrous ethanol in a 1:2 ratio.

2.3. Preparation, treatment, and storage of oysters

Fresh Rushan oysters were sourced from the seafood market in Qingdao City, Shandong Province. Oysters were selected post-shucking based on uniform morphology (10–15 cm length, 120–180 g weight) and fresh hay-like aroma. After thorough rinsing with purified water to eliminate surface contaminants, samples were packaged in sterile polypropylene vessels. Experiments on oyster freshness preservation were conducted using solutions with varying compositions: CTS, 0.05 % PC/CTS, 0.1 % PC/CTS, 0.2 % PC/CTS, and 0.4 % PC/CTS. Distilled water was used as the negative control, while commercially formulated meat preservatives, including sodium tripolyphosphate, sodium diacetate, and streptozotocin lactate, served as the positive control. Oysters were stored at 4 °C for 12 days, during which photographs were taken with a smartphone camera to document changes in appearance and assess variations in oyster quality.

2.4. Characterization of oysters during storage

2.4.1. Sensory evaluation (odor, color, texture, and overall acceptability)

A sensory rating scale was developed based on the method ISO 8586–1 described by Yue et al. (Yue et al., 2020). Seven trained sensory evaluators assessed oysters based on four criteria: odor (fresh hay to strong fishy or putrid odors), color (creamy to light brown), texture (firm and elastic to loose and soft, lacking elasticity), and overall acceptability (very good to completely unacceptable). Each attribute was evaluated on a scale of 2–10. The inter-rater reliability analysis showed a Cohen's kappa coefficient exceeding 0.6 for key attributes, indicating substantial agreement among panelists.

2.4.2. pH

Briefly, 5 g of oyster homogenate was weighed and thoroughly homogenized in 45 mL of distilled water. The mixture was left to stand for 30 min, after which its pH was measured using a pH meter.

2.4.3. Total volatile basic nitrogen (TVB-N)

TVB-N content in oysters was determined using the national standard GB 5009.228–2016 trace diffusion method. Briefly, 5 g of oyster homogenate was transferred into a centrifuge tube containing 25 mL of purified water and vigorously agitated with a vortex oscillator to ensure uniform dispersion. The TVB-N content was expressed in mg/100 g.

2.4.4. Lipid oxidation

The changes in malondialdehyde (MDA) levels in oysters during refrigeration reflect the rate of lipid oxidation. The MDA content was determined following the method outlined in GB 5009.181–2016. Briefly, 5 g of oyster homogenate was mixed with 50 mL of a trichloroacetic acid (TCA) solution, and the samples were thoroughly dispersed using a vortex oscillator. The results were expressed as mg MDA/100 g of sample.

2.4.5. Total bacterial count

The total bacterial count was determined following the GB 4789.2–2016 standard. Briefly, 5 g of oyster homogenate was weighed under aseptic conditions and placed in a sterile bag containing 45 mL of 0.9 % saline. The mixture was homogenized for 2 min to ensure uniform dispersion. Subsequently, 1 mL of the upper clear solution was collected in a test tube, and the total number of colonies was determined using plate count agar. The solution was diluted in a gradient with 0.9 % saline according to the decimal system and incubated at 28 °C for 48 h.

2.4.6. Changes in protein and lipid oxidation

Based on the above results, four representative groups (CTS, 0.05 % PC/CTS, 0.1 % PC/CTS, and NC) were selected for further analysis to evaluate their treatment effects on oyster quality and variation patterns.

2.4.6.1. Protein sulfhydryl (SH) content. The SH content was measured using a commercial assay kit (Nanjing Jiancheng Bioengineering Institute, China), following the manufacturer's instructions. A 2.0 g sample was mixed with 10 mL of 50 mmol/L phosphate buffer (pH 8.0) in a 50-mL centrifuge tube. The SH content was then calculated using the provided equation and expressed as μmol/g prot.

2.4.6.2. Protein hydrophobicity. The surface hydrophobicity was determined using the method described by Wang et al. (Wang et al., 2023). Briefly, 1 mL of oyster protein homogenate was centrifuged at 10,000 rpm for 5 min to obtain the supernatant. After mixing 1 mL of PBS (20 mmol/L, pH 6.0) and 80 μL of BPB (1 mg/mL) with the supernatant, the mixture was centrifuged again at 10,000 rpm for 15 min. The resulting supernatant was diluted with 2 mL of deionized water, and its absorbance at 595 nm (A_1) was recorded. A blank sample, prepared with BPB and PBS, was similarly diluted, and its absorbance (A_0) was measured. The surface hydrophobicity was then calculated using the following equation:

$$\textit{Bromophenol blue binding amount}\ (\mu g) = \frac{200 \times (A_0 - A_1)}{A_0} \quad (4)$$

2.4.6.3. Protein carbonyl. The carbonyl content was measured with slight modifications to the method described by Wang et al. (Wang et al., 2023). Briefly, 1 mL of oyster homogenate was mixed with 2 mL of 10 mM DNPH in 2 M HCl and incubated at 37 °C for 1 h in the dark. After adding 2 mL of 20 % TCA, the mixture was centrifuged at 12,000 rpm for 15 min at 4 °C to collect the precipitate. The precipitate was washed three times with 5 mL of an ethanol/ethyl acetate solution (1:1, *v*/v). The precipitate was then dissolved in 5 mL of 6 M guanidine hydrochloride (prepared in 2 M HCl) and incubated at 37 °C for 15 min. After centrifugation at 12,000 rpm at 4 °C, the supernatant was collected, and its absorbance was measured at 370 nm. The carbonyl content was then calculated and expressed as μmol/mg protein.

2.4.6.4. Lipid hydroperoxide (LPO) determination. LPO content was measured using a commercial assay kit (Beijing Boxbio Science & Technology Co., Ltd., China). A 0.1 g sample of oyster homogenate was mixed with 1 mL of PBS (pH 7.4) and homogenized. The LPO content was determined according to the manufacturer's instructions and calculated using the standard curve.

2.5. Statistical analysis

Statistical analyses were performed using one-way analysis of variance (ANOVA) to compare differences between groups. Post-hoc comparisons were conducted using Duncan's multiple range test to determine significant differences among the groups. A *p*-value of less than 0.05 was considered statistically significant. Each experiment was performed in triplicate to ensure the reliability and reproducibility of the results, and the average values were reported.

3. Results and discussion

3.1. Characterization of PC/CTS solution

3.1.1. Color, transparency, pH, PDI, particle size, and zeta potential

Table 1 shows that in the CTS/PC composite solution, the L*, a*, and b* values significantly decreased ($p < 0.05$) with increasing PC content. A higher PC addition resulted in a significant ($p < 0.05$) reduction in L*, while ΔE* increased considerably, indicating decreased brightness and greater color variation. The more negative a* and b* values suggest a shift toward green and blue hues, respectively. Additionally, light transmittance decreased significantly ($p < 0.05$), likely due to the interaction between CTS and PC, resulting in a more compact substance.

Table 1 presents the pH, PDI, particle size, and zeta potential of the composite solution. The composite solution exhibited significant acidity ($p < 0.05$), with the CTS group being the most acidic. In the acidic environment, CTS had a greater positive charge, with a pH of 2.31 ± 0.03. The pH of the composite solution increased slightly with increasing PC addition, likely because the basic groups (e.g., amino groups) in PC can accept protons. A significant difference in pH ($p < 0.05$) was observed at 2.59 ± 0.11 when PC addition reached 0.2 %. The negative charge of PC interacts with the positive charge of CTS, thereby reducing the concentration of free hydrogen ions in the solution.

The PDI reflects the degree of homogeneity in particle size, with a lower PDI indicating a more uniform particle size and more stable solution properties. As shown in Table 1, the PDI of the composite solution was significantly affected ($p < 0.05$) by the addition of PC. This effect is likely due to the increased intermolecular repulsion among the particles within the composite solution, leading to a more uniform particle distribution. As PC addition increased, the PDI of the composite solution decreased significantly ($p < 0.05$), with the final composite solution exhibiting a PDI of 0.30 ± 0.01.

The particle size of CTS was 826.05 ± 18.03 nm. With increasing PC content, the particle size expanded, suggesting that PC promoted complex aggregation, with higher concentrations potentially enhancing aggregation or crosslinking. Electrostatic interactions and hydrogen bonding facilitated the attachment of PC to CTS, leading to the formation of composite particles. At 0.1 % PC, the particle size increased significantly ($p < 0.05$) to 1147 ± 26.87 nm compared to that of the control. The largest particle size (1539.7 ± 55.15 nm) was observed

Table 1
Color, opacity, pH, polydispersity index, particle size, and zeta potential of all solutions.

		Solution				
		CTS	0.05 % PC/CTS	0.1 % PC/CTS	0.2 % PC/CTS	0.4 % PC/CTS
Color	L*	95.94 ± 0.01^{a}	94.97 ± 0.17^{b}	92.47 ± 0.09^{c}	85.45 ± 0.45^{d}	76.09 ± 0.33^{e}
	a*	-0.34 ± 0.02^{a}	-4.30 ± 0.17^{b}	-6.17 ± 0.12^{c}	-12.71 ± 0.40^{d}	-27.66 ± 0.15^{e}
	b*	-0.73 ± 0.09^{a}	-1.81 ± 0.09^{b}	-4.38 ± 0.05^{c}	-7.61 ± 0.12^{d}	-15.28 ± 0.16^{e}
	ΔE*	1.15 ± 0.02^{e}	4.88 ± 0.28^{d}	7.75 ± 0.15^{c}	17.69 ± 0.65^{b}	35.21 ± 0.34^{a}
Opacity (mm^{-1})		0.89 ± 0.08^{e}	1.66 ± 0.09^{d}	2.20 ± 0.16^{c}	3.01 ± 0.02^{b}	5.34 ± 0.30^{a}
pH		2.31 ± 0.03^{c}	2.43 ± 0.06^{bc}	2.47 ± 0.42^{bc}	2.59 ± 0.11^{a}	2.60 ± 0.11^{a}
PDI		0.78 ± 0.02^{a}	0.75 ± 0.01^{b}	0.46 ± 0.01^{c}	0.36 ± 0.02^{d}	0.30 ± 0.01^{e}
Particle size (nm)		826.05 ± 18.03^{d}	865.65 ± 31.61^{d}	1147.00 ± 26.87^{c}	1309.00 ± 32.53^{b}	1539.00 ± 55.15^{a}
Zeta potential (mV)		37.50 ± 2.55^{b}	39.23 ± 1.17^{b}	43.47 ± 0.83^{a}	42.13 ± 0.55^{a}	41.90 ± 1.35^{a}
Secondary structure	α-helix	0.091 ± 0.002^{b}	0.107 ± 0.002^{a}	0.049 ± 0.006^{e}	0.070 ± 0.004^{c}	0.057 ± 0.007^{d}
	β-sheet	0.392 ± 0.005^{b}	0.389 ± 0.004^{b}	0.413 ± 0.006^{a}	0.378 ± 0.002^{c}	0.380 ± 0.007^{c}
	β-turn	0.115 ± 0.007^{c}	0.115 ± 0.002^{c}	0.132 ± 0.004^{b}	0.130 ± 0.005^{b}	0.140 ± 0.004^{a}
	random coil	0.402 ± 0.005^{c}	0.389 ± 0.004^{d}	0.406 ± 0.006^{b}	0.422 ± 0.004^{a}	0.423 ± 0.002^{a}

Note: Different lowercase letters (a–e) in the same column indicate statistically significant differences among groups ($p < 0.05$) according to Duncan's multiple range test. Groups sharing the same letter are not significantly different. ΔE* represents total color difference (dimensionless); PDI represents polydispersity index (dimensionless); secondary structure parameters are expressed as relative proportions.

with an addition of 0.4 % PC.

CTS, being a cationic molecule, exhibited a positive zeta potential of 37.5 ± 2.55 mV in the absence of PC. As the pH of the composite solution was below the isoelectric point of PC, the amino acid side chains of PC were protonated, resulting in a net positive charge. In the system of the two complexes, the solution exhibits the cationic nature of the polymer, thereby increasing the potential. At PC additions up to 0.1 %, the positive charge superposition in the solution increased the potential, with a significant change in zeta potential ($p < 0.05$) recorded at 43.47 ± 0.83 mV. However, at higher PC concentrations, the zeta potential stabilized, likely owing to the electrostatic repulsion between PC and CTS, with minor negative charges from PC partially neutralizing CTS.

3.1.2. FTIR spectroscopy

FTIR analysis was conducted to examine the interaction between different PC concentrations and the matrix CTS. As shown in Figure 1 (A), the PC spectrum exhibits a distinct peak at 2927.41 cm^{-1}, attributed to C–O–H vibrations and symmetric and asymmetric C—H stretching (Wang et al., 2022). Additionally, distinct peaks at 1656.55 and 1548.55 cm^{-1} correspond to amides I and II, respectively. The composite spectra closely resembled those of CTS, suggesting the dominant role of CTS in PC/CTS interactions. Shifts in peak intensity and wavenumber with increasing PC concentrations suggest interactions between the carboxyl/carbonyl groups of PC and hydroxyl/amide groups of CTS. At 0.2 % PC, the peak intensity reached its maximum, suggesting enhanced bonding. The distinctive peak at 3421.10 cm^{-1} is attributed to the O—H stretching vibration (Jiang & Zheng, 2023). Upon PC addition, the O—H stretching peak at 3421.10 cm^{-1} exhibited a redshift, further suggesting the presence of hydrogen bonding. The characteristic peak at 1716.34 cm^{-1} is attributed to the stretching vibration of C═O. Peaks at 1396.21 cm^{-1} (C–OH), 1220.72 cm^{-1} (C–O–C), and 1085.73 cm^{-1} (C—O) indicate potential hydrophobic interactions between PC and CTS, likely due to the abundance of hydrophobic groups in this region.

3.1.3. CD spectroscopy

As shown in Figure 1(B), CTS exhibited a distinct negative peak at 210 nm in the far-ultraviolet region, indicating the presence of an internal α-helical structure. Pure PC exhibited a negative peak at 220 nm, while the composite solution initially maintained a negative peak at 210 nm with low PC addition, shifting to 215.5 nm when the PC content reached 0.4 %. Table 1 illustrates the proportion of protein secondary structures in the composite solution. The α-helical content initially increased with PC addition, reaching its peak at 10.7 % at 0.05 % PC ($p < 0.05$), which suggests the highest structural order. As PC concentrations approached 0.2 %, the protein structures shifted from α-helices and β-folds to β-turns and irregular curls, resulting in a more disordered configuration.

3.1.4. Viscosity

Figure 1(C) shows the fluctuations in the rheological characteristics of the composite solution at shear rates ranging from 0.1 to 100 s^{-1}. The viscosity of the composite solution was significantly higher than that of ultrapure water, with CTS exhibiting the highest viscosity, which decreased to 186.63 Pa·s at 100 s^{-1}. Furthermore, the viscosity of the composite solution decreased with increasing PC content. The high viscosity of CTS is due to the interactions of hydroxyl, amino, and *N*-acetylamino groups along its macromolecular chain, which result in the formation of diverse intramolecular and intermolecular hydrogen bonds. Upon the addition of PC, the viscosity decreases because the positive charge of PC electrostatically repels the positive charge of the amino groups in CTS. Increased viscosity positively impacts food preservation by enhancing the protective barrier around the food. Costa et al. (Costa et al., 2014) used sodium alginate, an anionic polysaccharide characterized by polyhydroxyl and carboxyl groups, to immerse oysters. By leveraging the weak gelation and film-forming properties of sodium alginate, a preservation gel was formed on the surface of oysters. This approach improved the uniformity and durability of preservation while maintaining the texture and flavor of the oysters.

3.1.5. XRD

XRD analysis can determine the crystal structure of composite films formed by different concentrations of PC and CTS. As shown in Figure 1 (D), PC/CTS exhibited a semi-crystalline nature, reflecting the amorphous characteristics of the polymer. The peak morphologies remained largely consistent across all groups, each showing a dominant peak within the range of $2\theta = 20.43°–22.19°$, suggesting a homogeneous mixture and robust structural integrity (Akhtar, Zhao, Li, & Shi, 2024). The control CTS exhibited the highest characteristic peak intensity, suggesting a greater abundance of hydroxyl groups, a more stable internal molecular architecture, a high degree of crystallization, the largest grain size, and the highest amount of crystalline phases. The incorporation of PC caused a noticeable alteration in the highest point of the primary peak in the XRD pattern of the composite membrane, suggesting enhanced interactions between the hydrogen bonds and hydrophobic interactions of PC and CTS.

3.1.6. Antibacterial activity evaluation

The filter paper sheet method was used to evaluate the inhibitory activity of the composite solution against *P. aeruginosa* and total oyster-rotting bacteria. According to Cao et al. (Cao, Xue, & Liu, 2009), *P. aeruginosa* is the predominant spoilage bacterium in oysters at various refrigeration temperatures, with its proportion reaching 73 % by the end of storage. The composite solution exhibited strong inhibitory effects on *P. aeruginosa* and total oyster-rotting bacteria. Figure 1(E) shows the range of inhibition zone diameters created by composite solutions of different compositions on *P. aeruginosa*. Notably, the 0.05 % PC/CTS solution demonstrated optimal inhibition of *P. aeruginosa*, with an inhibition circle diameter of 21.03 ± 0.55 mm (Figure 1(G)). Figure 1(F) shows the inhibitory effects against total oyster spoilage bacteria, with CTS alone exhibiting the most potent activity, producing an inhibition zone of 23.65 ± 0.77 mm (Figure 1(H)). CTS possesses broad-spectrum bacteriostatic properties. Its mode of action involves the cationic charge of CTS interacting with the negatively charged cell surface, leading to nutrient leakage. The bacteriostatic properties of the composite solution increased and then significantly decreased ($p < 0.05$) with increasing PC content, suggesting that PC possesses some bacteriostatic properties against *P. aeruginosa* in oyster spoilage bacteria. However, as the PC concentration increased, the antibacterial effect of the composite decreased, possibly due to the formation of larger aggregates, as evidenced by particle size analysis (Table 1). Specifically, the particle size of the composite solution increased with higher PC concentrations, potentially hindering CTS from effectively interacting with bacterial membranes. SEM analysis further revealed that at lower PC concentrations (0.05 % and 0.1 %), the complexes maintained a smooth, uniform structure, promoting stable interactions between CTS and PC. However, at higher PC concentrations, the internal structure and surface of the complexes developed porosity and inhomogeneous patches, which may disrupt the structural integrity and reduce the bacteriostatic efficacy of the composite.

3.1.7. SEM and contact angle of PC/CTS solution

As shown in Figure 2(a), When PC is not added, CTS exhibits a smooth, uniform structure. The micro-morphology of the composite with 0.05 % and 0.1 % PC addition maintained a flat and smooth appearance, suggesting that stable structures were formed through interactions between PC and CTS. However, at higher PC concentrations, the internal structure and surface of the complexes became porous and inhomogeneous, indicating that excessive PC disrupts structural integrity and reduces the stability of the composite.

Previous studies have shown that CTS and PC are generally considered hydrophilic (Li, Li, & Abbaspourrad, 2024). Nonetheless,

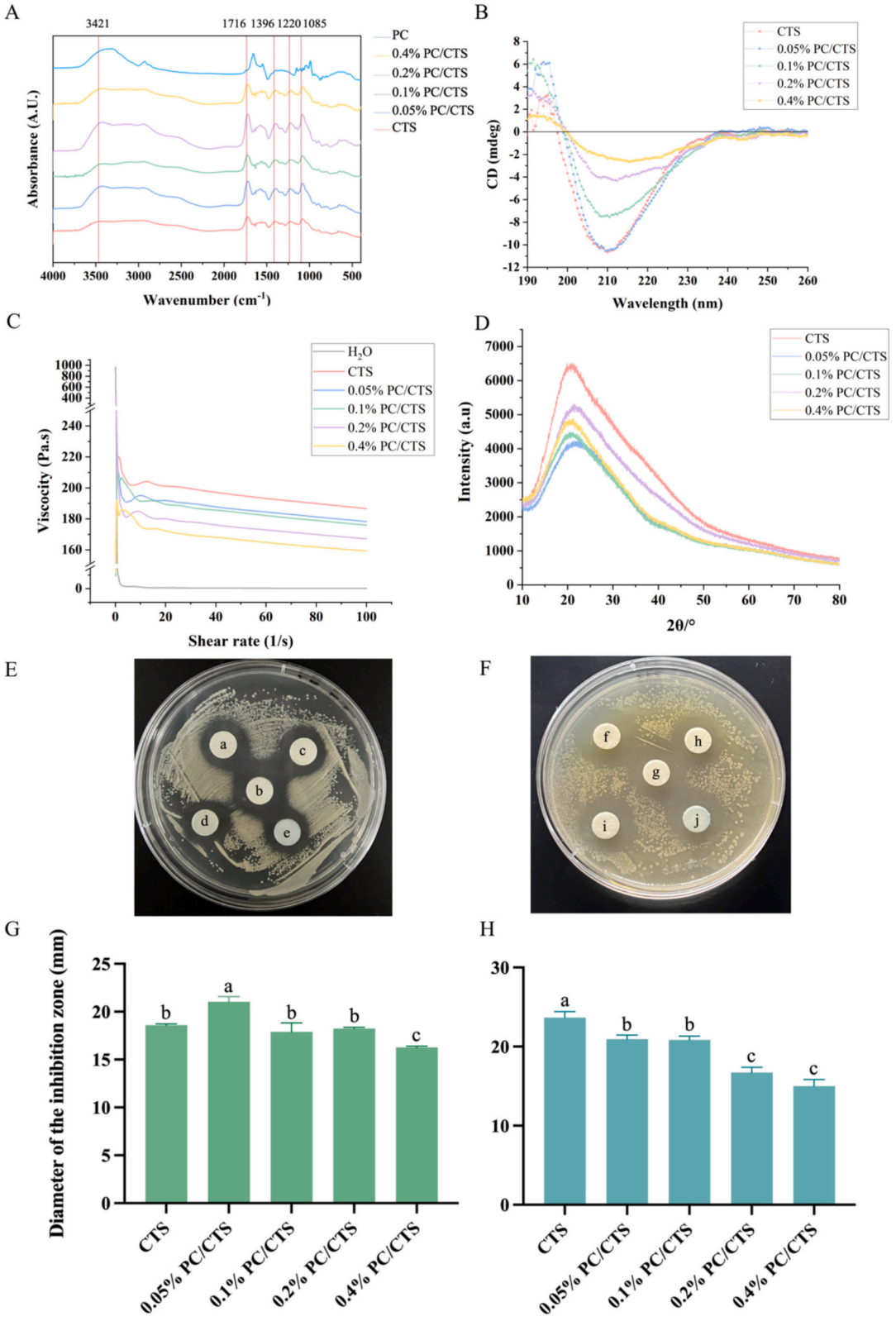

Figure 1. Infrared spectrogram of the composite solution (A). Circular dichroism (B). Viscosity and rheological properties of the composite solution (C). X-ray diffraction patterns (D). Antimicrobial activity images showing inhibition zones for different solutions: (E) *Pseudomonas aeruginosa* and (F) total oyster spoilage bacteria (TSB). Diameters of inhibition zones for (G) *P. aeruginosa* and (H) TSB: (a) CTS, (b) 0.05 % PC/CTS, (c) 0.1 % PC/CTS, (d) 0.2 % PC/CTS, (e) 0.4 % PC/CTS, (f) CTS, (g) 0.05 % PC/CTS, (h) 0.1 % PC/CTS, (i) 0.2 % PC/CTS, (j) 0.4 % PC/CTS.

0.4% PC/CTS, (f) CTS, (g) 0.05% PC/CTS, (h) 0.1% PC/CTS, (i) 0.2% PC/CTS, (j) 0.4%

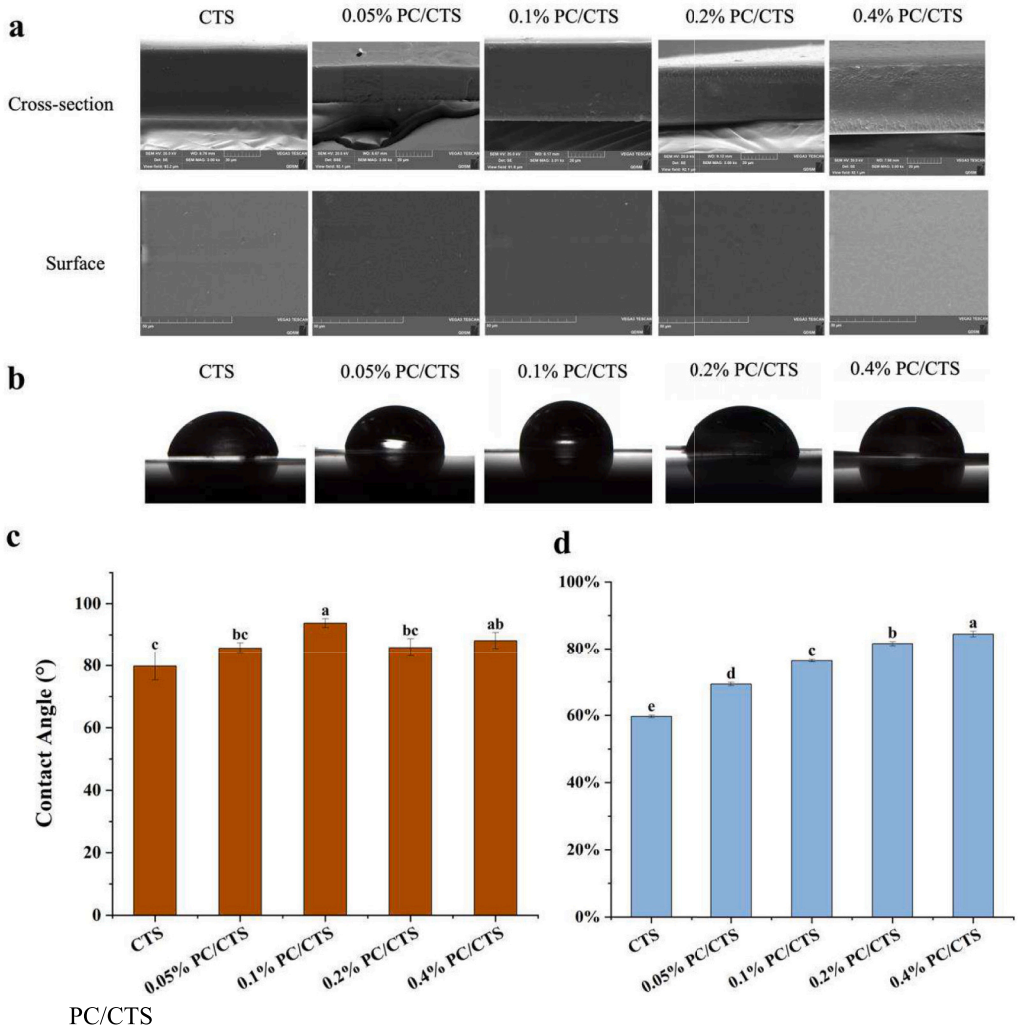

Figure 2. Composite solution after drying: (a) Scanning electron microscopy image, (b) contact angle measurement image, (c) contact angle experimental results, and (d) DPPH radical scavenging activity.

experimental results revealed that CTS solution exhibited the highest hydrophilicity, with a contact angle of 79.80° ± 4.46° (Figure 2(b)). Upon the addition of PC, the hydrophobicity of the composite solution was significantly enhanced ($p < 0.05$), peaking at 0.1 % PC with a contact angle of 93.81° ± 1.42° (Figure 2(c)). Based on the IR results, it is speculated that the composite solution adopts a structure where PC is encapsulated and CTS forms an outer layer. The hydrophilic groups of CTS interact internally with PC, while the hydrophobic groups extend outward, resulting in the folding of O—H and N—H groups within the protein. The enhanced hydrophobicity of the complexes improves their barrier properties in food preservation, reducing the adverse effects of water molecules. (Feng, Sun, Zhao, Li, & Ju, 2025). However, excessive hydrophobicity may reduce the dispersion of the composite solution in aqueous environments, potentially weakening its interaction with bacterial cells.

3.1.8. DPPH scavenging effect

PC, as a biomolecule with antioxidant activity, can scavenge superoxide radicals, hydroxyl radicals, peroxyl radicals, H_2O_2, and HClO. As shown in Figure 2(d), the free radical scavenging capacity of the composite solution significantly increased ($p < 0.05$) with the continuous addition of PC. With 0.4 % PC addition, the free radical scavenging capacity reached 84.27 %, which was considerably higher than that observed in the CTS group (59.70 %). Pure PC fibers scavenged 17.68 % DPPH free radicals, which was 1.4 times higher than that of pure PVA fibers (Zhang et al., 2023). The fundamental antioxidant component of PC is PCB, which demonstrates antioxidant activity comparable to that of other tetrapyrroles (e.g., bilirubin). Radomirovic et al. (Radomirovic et al., 2022) demonstrated that the β-lactoglobulin (BLG)–PCB complex exhibits enhanced antioxidant capabilities, with the attached PCB protecting BLG from free radical–stimulated oxidation. The molecular structure of CTS contains many active groups, including hydroxyl and amino groups, which confer its free radical scavenging properties and effectively prolong the antioxidant activity of the solution.

3.2. Effect of the composite solution on refrigerated Rushan oysters

3.2.1. Sensory evaluation

3.2.1.1. Color. Figure 3 shows the appearance changes in oysters during storage. Fresh oysters display creamy white glands and dark brown skirts with a bright luster. Initially, the color differences between the experimental and control groups were not significant ($p > 0.05$). However, as the preservation time extends, oxidation and microbial activity

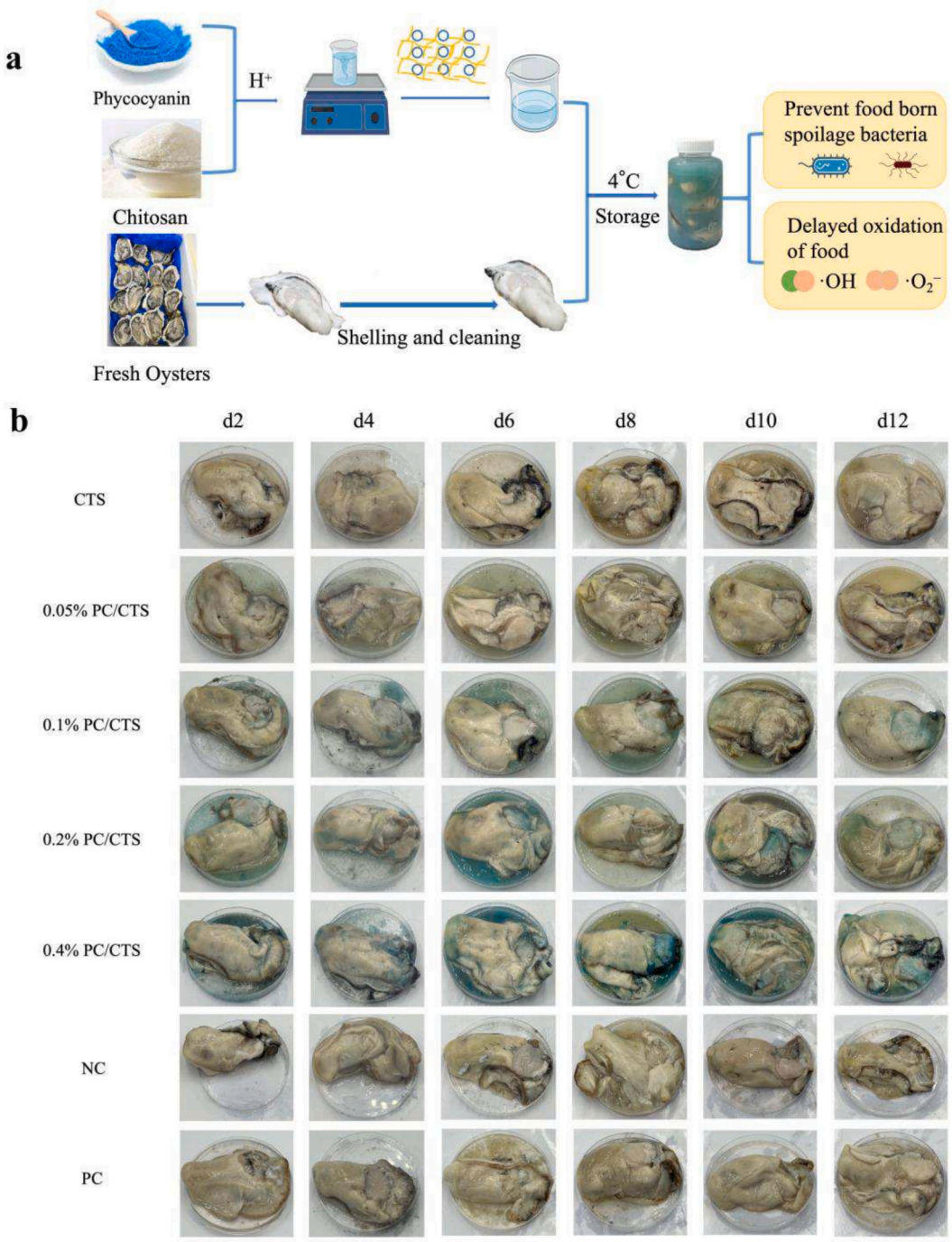

Figure 3. Schematic diagram illustrating the preparation process of the phycocyanin/chitosan composite solution and its application to oyster cold storage (a). Changes in the appearance of oysters during refrigeration under different treatment conditions (b).

cause content leakage, tissue shrinkage, and discoloration, with the glands turning yellow and brown and the adductor muscle becoming darker and duller. The color of the negative control group significantly darkened ($p < 0.05$) on day 6, followed by the positive control group on day 8. By day 10, some sections started to brown due to the natural deterioration of the oysters (Figure 4(a)). In the experimental group, the oysters exhibited a lighter color on days 4 and 6, which may be attributed to the antioxidant properties of PC. After day 8, intensified microbial activity, along with increased lipid oxidation and protein denaturation, led to progressive darkening of the oyster tissues. These findings indicate that while PC may initially slow color deterioration, its protective effect diminishes as microbial activity and oxidative processes advance beyond day 8.

3.2.1.2. Odor. Fresh oysters possess the flavor of fresh licorice. However, with increasing storage time, their muscle protein progressively denatures and degrades, fat gradually oxidizes, and cell structure undergoes autolysis. Eventually, they develop a strong fishy odor and rotten taste. The odor scores of the negative controls declined rapidly during storage (Figure 4(b)), with a detectable sour odor emerging on day 2, intensifying by day 4, and developing into a pronounced sour and decaying odor after day 6. The positive control group exhibited a mildly irritating odor from the oysters on day 6, which developed into a strong, irritating chemical odor by day 8. This odor may be attributed to the

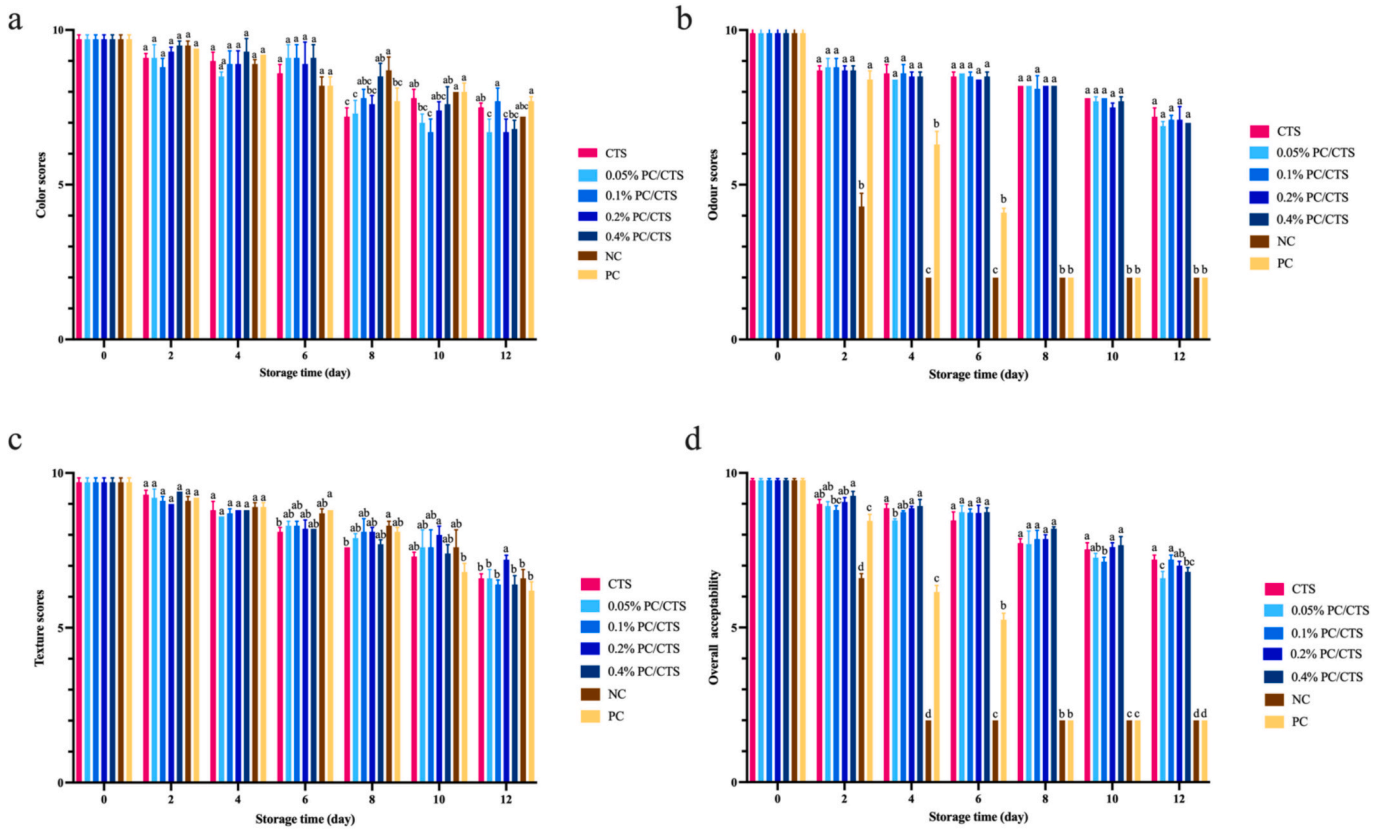

Figure 4. Effect of different treatments on the quality of oysters during cold storage: (a) odor, (b) color, (c) texture, and (d) overall acceptability. Scoring criteria: odor—10: licorice flavor, 8: seaweed flavor, 6: strong seaweed flavor with slight odor, 4: noticeable odor with fishy smell, 2: strong fishy or rotting smell; color—10: creamy, 8: white, 6: light yellow, 4: yellow, 2: light brown; texture—10: firm, elastic, and full to the touch, 8: firmer and slightly elastic, 6: slightly soft and not firm, 4: soft with poor elasticity, 2: loose, softened, and non-elastic; overall acceptability—10: very good, 8: better, 6: average, 4: worse, 2: totally unacceptable.

chemicals present in commercially available preservatives. Conversely, the negative control group began emitting an unpleasant sour odor from day 2, and the positive control group developed odors from day 4. Moreover, the experimental group's odor transitioned more smoothly over the storage period, evolving from a licorice-like flavor to a stronger seaweed aroma. The odor scores of the experimental group showed a substantial decline after day 10, accompanied by an increase in the intensity of the seaweed odor. By day 12, the odor scores of the experimental group were significantly higher than those of the negative and positive control groups. The odor score of CTS was 7.2, which was not significantly different ($p > 0.05$) from the other groups within the experimental group.

3.2.1.3. Texture. The flesh of fresh oysters is firm, springy, and substantial to the touch. However, as refrigeration time increases, autolytic enzymes (including lipase and protease) become activated and progressively break down the cellular structure of the oysters. This process causes the tissues to gradually lose water, resulting in softer, looser, and less elastic meat. At the beginning of the preservation experiment, there was no discernible difference in the texture of oysters. Nonetheless, by day 6, the oysters in the experimental group exhibited less hardness than those in the negative and positive control groups (Figure 4(c)). This may have been due to the acidic conditions and bacteriostatic properties, which adversely affected the outer surface tissues of the oysters. The texture scores were higher in the negative and positive control groups from days 0 to 6. Nevertheless, by day 8, the oysters' texture showed increased softness, reduced elasticity, diminished tissue thickness, and enhanced visibility of internal brown microalgae on the surface. These findings suggest that polysaccharides, such as extracellular polysaccharides, are produced concurrently with the growth of spoilage bacteria, resulting in a sticky, slick texture on the oyster surface.

3.2.1.4. Overall acceptability. Figure 4(d) shows the change in the overall acceptability of oysters during cold storage under different treatment modes. The negative control group experienced the most rapid decline in overall acceptability during refrigeration, with the score dropping from 6.7 on day 4 to a significant ($p < 0.05$) decrease of 2 by day 6, likely due to the production of sour and spoilage aromas at that time. The overall acceptability score in the positive control group decreased to 5.2 by day 8, likely due to the strong irritating and chemical odors detected on that day. By day 12, the overall acceptability scores of the experimental groups remained above 6, with no significant differences ($p > 0.05$) observed between the groups. The relatively high acceptance of the experimental groups suggests that the blue hue of the solution was not a major determinant in sensory evaluation, with attributes such as odor and texture playing a more dominant role in overall acceptability.

3.2.2. pH

Figure 5(a) shows the pH changes during the storage of oysters at 4 °C. The pH of fresh oysters was initially 5.88 and decreased in the negative control group as storage time progressed. By day 2, the pH of

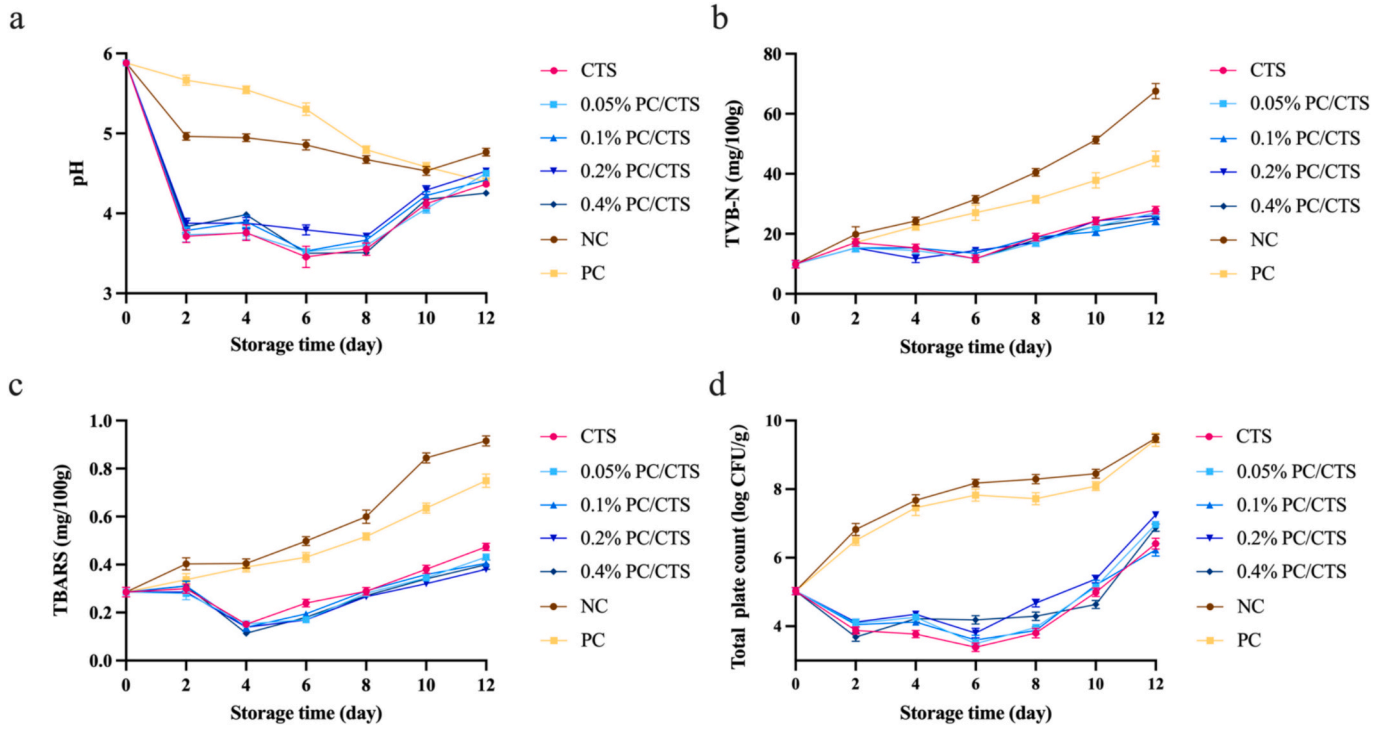

Figure 5. Changes in (a) pH, (b) volatile basic nitrogen, (c) thiobarbituric acid reactive substances, and (d) total plate count of oysters during refrigeration under different treatments.

oysters dropped to 4.97, primarily due to increased bacterial activity, the production of lactic acid and acetic acid through microbial metabolism, and the breakdown of sugars in the muscle tissue. From days 2 to 10, the pH continued to drop as spoilage bacteria proliferated extensively, producing more organic acids and metabolites in the negative control group. After day 10, proteolysis led to the release of alkaline compounds such as trimethylamine (TMA), amino acids, and ammonia, resulting in a pH rebound. This pH increase may be influenced by protein degradation processes, including the oxidation of protein components (e.g., thiol and carbonyl groups) and changes in protein hydrophobicity, which are further elaborated in Section 3.2.6. The positive control group delayed the reduction in pH, suggesting its potential in slowing down the spoilage process in oysters. In the experimental groups, a rapid decrease in pH occurred from days 0 to 2, reaching 3.72 in the CTS group due to its intrinsic acidity. The quality of oysters started to decline substantially after day 8, coinciding with a significant increase ($p < 0.05$) in pH observed in the experimental groups. By the end of the storage period, the pH of the experimental groups and positive control group was significantly lower ($p < 0.05$) than that of the negative control group, suggesting enhanced preservation effects.

3.2.3. TVB-n

TVB-N is a key indicator of protein degradation in oysters. During prolonged refrigeration, the gradual breakdown of proteins in oysters results in the accumulation of amino acids, amines, and other degradation products, including basic nitrogen compounds such as TMA, dimethylamine, and ammonia (Cao, Xue, Liu and Xue, 2009). Figure 5 (b) shows the fluctuations in TVB-N values of oysters during cool storage. The initial TVB-N value of raw oysters was 9.9 mg/100 g. After 2 days of storage, the TVB-N values of all groups increased significantly ($p < 0.05$). The negative control group exhibited the highest TVB-N value on day 4, which was significantly different ($p < 0.05$) from the other groups. The positive control group showed a relatively slower rate of increase in TVB-N values. In contrast, the experimental group displayed a declining trend, likely due to the high adsorption capacity of CTS, which absorbs basic nitrogen compounds into the solution. Similar mechanisms have been observed in previous studies, where amino groups in polymeric matrices were found to cross-link with hydroxyl and carboxyl groups in bioactive molecules, thereby affecting their stability and retention (Ran et al., 2021). Additionally, the strong antibacterial properties of CTS inhibit microbial growth and metabolism, thereby reducing the production of alkaline substances such as ammonia and amines. The negative control group reached a TVB-N value of 31.5 mg/100 g on day 6, exceeding the threshold for determining oyster freshness (TVB-N content within 30.0 mg/100 g) (Siddiqui, Singh, Bahmid, & Sasidharan, 2024). On day 12, the 0.1 % PC/CTS group recorded the lowest TVB-N value at 24.3 mg/100 g. The increase in TVB-N values observed with the continuous addition of PC may be due to partial degradation of PC itself.

3.2.4. Lipid oxidation

Autoxidation is generally initiated by the interaction of oxygen with hydrogen atoms on the methylene groups of unsaturated fatty acids. Although oysters have a low fat content, their fats—particularly polyunsaturated fatty acids—are highly susceptible to oxidation during refrigeration, resulting in the formation of peroxides and secondary metabolites such as MDA. Figure 5(c) shows the changes in thiobarbituric acid reactive substances (TBARS) values of oysters during cold storage. Fresh oysters have a TBARS value of 0.29 mg/100 g. During the initial storage period, TBARS values in the positive and negative control groups increased at a slower rate, likely due to the suppression of oxidative reactions at low temperatures. However, as the refrigeration period progresses, the lipids in oysters gradually oxidize, leading to the development of off flavors. The TBARS values of the experimental groups exhibited an initial decline, reaching a minimum on day 4, followed by an increase. In contrast, the TBARS values of the other groups gradually increased as the PC concentration decreased. This demonstrates that PC acts as a potent antioxidant, inhibiting the autoxidation and enzymatic oxidation of lipids during oyster refrigeration. This observation is supported by experiments conducted by Li et al. (Li, Li, & Abbaspourrad, 2024), which showed that PC was initially

targeted in the system, thereby delaying the oxidation of the PC–urea emulsion. Furthermore, CTS in the composite solution possesses high viscosity and gel properties. By binding with microorganisms and lipids on oyster surfaces, it forms a protective film that shields oysters from oxygen exposure and creates a reducing environment on their surface and within their tissues. The antioxidant advantage of 0.4 % PC/CTS slightly decreased after day 6, which may be attributed to the oxidation and degradation of PC during storage.

3.2.5. Total bacterial count

Although most pathogenic bacteria are inhibited at a refrigeration temperature of 4 °C, some psychrophilic bacteria, such as *P. aeruginosa*, a specific spoilage organism in oysters, can still grow slowly at low temperatures, accelerating the deterioration and spoilage process of oysters (Wang et al., 2023). Figure 5(d) shows the changes in the aerobic plate count (APC) of oysters stored at 4 °C under different treatments. The initial colony total of oysters was 5.03 log CFU/g. Between days 0 and 2, the colony total in the negative control group increased significantly ($p < 0.05$), reaching 6.83 log CFU/g. After day 10, the colony total showed another significant increase ($p < 0.05$), rising to 9.49 log CFU/g by day 12. The positive control group exhibited a significant difference compared to the negative control group only between days 8 and 10, suggesting limited inhibitory effects on the dominant spoilage bacteria. The trend in the experimental group initially showed a decline, reaching the lowest count on day 6, followed by a significant ($p < 0.05$) increase between days 10 and 12. This suggests that CTS and PC exhibited a stronger inhibitory effect on oyster spoilage bacteria and effectively reduced the initial bacterial load formed in fresh oysters exposed to air after treatment. Early in the preservation process, the CTS group's total oyster colony count remained low, reaching 3.39 log CFU/g on day 6, which was significantly different ($p < 0.05$) from the other experimental groups. However, as storage progressed, the bacteriostatic effect of PC became more pronounced. By day 12, the 0.1 % PC/CTS group recorded the lowest APC value (6.23 log CFU/g), which was significantly lower ($p < 0.05$) than the values of other groups and remained below the acceptable limit of 7.00 log CFU/g (Min et al., 2020). These findings suggest that PC exhibits strong oxidizing and bacteriostatic properties, while CTS offers broad-spectrum bacteriostatic effects by interacting with anions on bacterial cells and disrupting cell structure. Additionally, the acidic nature of the composite solution contributed to bacterial inhibition. Furthermore, the composite solution likely formed a protective layer around bacterial cells on the oyster surface, restricting gas and solute exchange and thereby inhibiting aerobic spoilage bacteria such as *P. aeruginosa* (Liu et al., 2023).

3.2.6. Changes in protein and lipid oxidation

3.2.6.1. Protein SH content. Thiol (–SH) groups in proteins readily oxidize into disulfide bonds (–S–S–) during storage, resulting in cysteine crosslinking or further oxidation into cysteine sulfonic acids. As shown in Figure 6(a), fresh oysters had a thiol content of 0.30 mmol/g prot, which significantly declined ($p < 0.05$) in the negative control group by day 2, decreasing further to 0.13 mmol/g prot on day 12. Protein oxidation progressed more slowly in the 0.1 % PC/CTS group; the 0.05 % PC/CTS group retained the highest thiol content after day 6, maintaining a level of 0.19 mmol/g prot on day 12. Lower PC concentrations were more effective in preserving thiol activity and protein stability during refrigeration. Protein oxidation occurs earlier than lipid

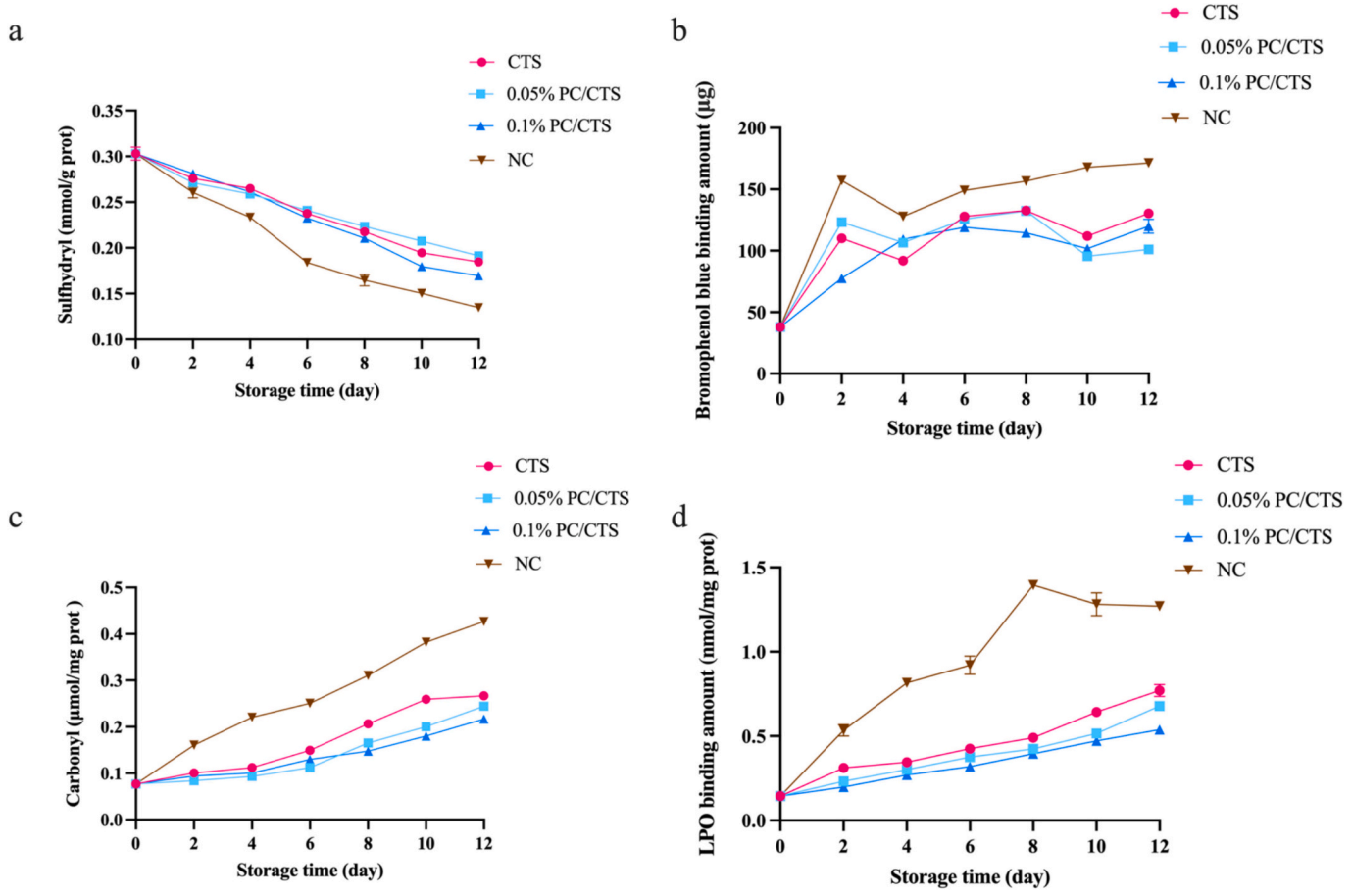

Figure 6. Changes in (a) protein thiol content, (b) protein surface hydrophobicity, (c) protein carbonyl content, and (d) lipid peroxidation levels of oysters during refrigeration under different treatments.

oxidation due to its higher susceptibility to free radicals (Münch et al., 2024). The 0.05 % PC formulation reduced oxidative stress by scavenging free radicals and limiting oxygen exposure, thereby delaying protein oxidation and slowing oyster quality deterioration. Additionally, CTS inhibited microbial activity, reducing protein degradation and minimizing thiol loss.

3.2.6.2. Protein hydrophobicity. Figure 6(b) shows that protein hydrophobicity in all groups reached its lowest point on day 4 before increasing, suggesting enhanced hydration on day 4 as water diffused onto the protein surface, reducing the exposure of hydrophobic domains. After day 4, the hydrophobicity in the control group increased, likely due to protein unfolding or denaturation, which exposed hydrophobic residues and softened the texture. On day 2, the 0.1 % PC/CTS group exhibited the lowest hydrophobicity (77.63 μg). After day 10, the 0.05 % PC/CTS group showed the lowest hydrophobicity (101.02 μg on day 12), possibly due to the prolonged protective effect of 0.05 % PC. The stronger interactions between 0.1 % PC and proteins may have induced conformational changes, leading to increased hydrophobicity. CTS likely stabilized the tertiary structure by binding to hydrophobic regions, enhancing protein–water interactions, and slowing the increase in hydrophobicity.

3.2.6.3. Protein carbonyl content. Carbonyl groups, formed through free radicals and peroxides, serve as indicators of protein oxidation severity. Figure 6(c) shows that fresh oysters had a carbonyl content of 0.077 μmol/mg prot. During refrigeration, the control group exhibited significantly higher carbonyl levels than the treatment groups ($p < 0.05$), with a general upward trend. The slower increase observed from days 4 to 6 suggests that spoilage involved additional degradation pathways. Moisture loss may have contributed to the increased ionic strength, thereby enhancing oxidation susceptibility (Gao et al., 2023). In the treatment groups, carbonyl levels remained stable until day 6, likely due to the protective effect of the composite solution. The 0.05 % PC/CTS group initially exhibited the slowest increase in carbonyl levels, while after day 6, the 0.1 % PC/CTS group had the lowest accumulation, reaching 0.22 μmol/mg prot on day 12. The synergistic effect of PC and CTS effectively reduced protein oxidation and slowed carbonyl accumulation.

3.2.6.4. LPO determination. LPO levels represent the concentration of free peroxides, suggesting the early stage of lipid oxidation in oysters. As shown in Figure 6(d), the control group displayed significantly higher LPO levels than the treatment groups, reaching a peak of 1.40 nmol/g prot on day 8, signifying the late stage of lipid oxidation. After day 8, LPO levels stabilized, likely owing to peroxide degradation into aldehydes, which can interact with cellular proteins, altering their structure and function and impacting food safety. In the treatment groups, LPO levels increased throughout the storage period, whereas the TBARS values initially declined before rising, reaching their lowest point on day 4. This suggests that from days 0 to 4, oysters were in the early oxidation stage, with peroxide accumulation progressing at a slow rate. Between days 4 and 6, the TBARS values started to rise, suggesting a transition to the mid-oxidation stage with intensified oxidative reactions. During the late refrigeration stage (days 8–12), LPO levels continued to increase, reaching 0.54 nmol/g prot in the 0.1 % PC/CTS group on day 12. At this stage, secondary oxidation products, such as MDA, accumulated, contributing to an increase in TBARS values. Additionally, free radicals generated by lipid oxidation may have induced polyphenol polymerization, exposing protein hydrophobic groups and darkening the oyster color.

4. Conclusions

The complexation of CTS with algal PC significantly enhanced the physicochemical properties of the solution. The incorporation of a moderate amount of PC imparted a bluish color, improved solution stability, and increased oxidation resistance compared to the control. The composite solution exhibited higher viscosity and enhanced bacteriostatic and hydrophobic properties, facilitating the formation of a more ordered internal structure. The PC/CTS treatment extended the shelf life of shucked oysters to 12 days under refrigeration compared to only 4 days for the untreated control. Oysters treated with the 0.1 % PC/CTS solution demonstrated a TVB-N value of 24.3 mg/100 g, TBARS value of 0.41 mg/100 g, and microbial count of 6.23 log CFU/g after 12 days of storage. Higher PC concentrations (0.2–0.4 %) were less effective, possibly due to disruption of the solution's structural integrity and reduced antibacterial efficacy. These results highlight the efficacy of the PC/CTS combination solution as a natural, safe, and effective method for preserving oysters and other perishable aquatic products during cold storage. To enable commercial adoption, subsequent studies should investigate scale-up considerations including production economics and long-term stability under industrial storage scenarios.

CRediT authorship contribution statement

Yan Li: Writing – original draft, Methodology, Formal analysis, Data curation, Conceptualization. **Li Liu:** Writing – review & editing, Project administration, Conceptualization. **Youwei Du:** Software, Methodology, Formal analysis. **Zihao Yin:** Supervision, Project administration, Methodology. **Yue Zhao:** Project administration, Formal analysis. **Guangxin Feng:** Writing – review & editing, Supervision, Data curation, Conceptualization. **Mingyong Zeng:** Writing – review & editing, Supervision, Resources, Funding acquisition, Formal analysis, Conceptualization.

Declaration of competing interest

The authors declare that they have no known competing financial interests or personal relationships that could have appeared to influence the work reported in this paper.

Appendix A. Supplementary data

Supplementary data to this article can be found online at https://doi.org/10.1016/j.fochx.2025.102456.

Data availability

The authors do not have permission to share data.

References

Akhtar, H. M. S., Zhao, Y., Li, L., & Shi, Q. (2024). Novel active composite films based on carboxymethyl cellulose and sodium alginate incorporated with phycocyanin: Physico-chemical, microstructural and antioxidant properties. *Food Hydrocolloids, 147*, Article 109440. https://doi.org/10.1016/j.foodhyd.2023.109440

Bergandi, L., Apprato, G., & Silvagno, F. (2022). Antioxidant and anti-inflammatory activity of combined Phycocyanin and Palmitoylethanolamide in human lung and prostate epithelial cells. *Antioxidants, 11*(2), 201. doi: 10/g8ps9s.

Cao, R., Xue, C., & Liu, Q. (2009). Changes in microbial flora of Pacific oysters (*Crassostrea gigas*) during refrigerated storage and its shelf-life extension by chitosan. *International Journal of Food Microbiology, 131*(2–3), 272–276. doi: 10/dr7bck.

Cao, R., Xue, C.-H., Liu, Q., & Xue, Y. (2009). Microbiological, chemical, and sensory assessment of Pacific oysters (*Crassostrea gigas*) stored at different temperatures. *Czech Journal of Food Sciences, 27*(2), 102–108. doi: 10/gs37b5.

Chand, A. (2024). *Seafood preservation strategies. Nature Food, 5*(4), 273. doi: 10/g8qrbh.

Chen, H., Guo, X., Yu, S., Meng, H., Ai, C., Song, S., & Zhu, B. (2024). Phycocyanin/tannic acid complex nanoparticles as Pickering stabilizer with synergistic interfacial antioxidant properties. *Food Chemistry, 434*, Article 137353.

Chini Zittelli, G., Lauceri, R., Faraloni, C., Silva Benavides, A. M., & Torzillo, G. (2023). Valuable pigments from microalgae: Phycobiliproteins, primary carotenoids, and fucoxanthin. *Photochemical & Photobiological Sciences, 22*, 1733–1789. https://doi.org/10.1007/s43630-023-00407-3

Costa, C., Conte, A., & Del Nobile, M. A. (2014). Effective preservation techniques to prolong the shelf life of ready-to-eat oysters: Prolonging the shelf life of ready-to-eat

oysters. *Journal of the Science of Food and Agriculture, 94*(13), 2661–2667. doi: 10/gs3r6g.
Feng, Z., Sun, P., Zhao, F., Li, M., & Ju, J. (2025). Advancements and challenges in biomimetic materials for food preservation: A review. *Food Chemistry, 463*, Article 141119. doi: 10/g8xrmk.
Gao, S., Liu, Y., Fu, Z., Zhang, H., Zhang, L., Li, B., Tan, Y., Hong, H., & Luo, Y. (2023). Uncovering quality changes of salted bighead carp fillets during frozen storage: The potential role of time-dependent protein denaturation and oxidation. *Food Chemistry, 414*, Article 135714. doi: 10/gr2mc5.
Golmakani, M.-T., Hajjari, M. M., Kiani, F., Sharif, N., & Hosseini, S. M. H. (2024). Application of electrospinning to fabricate phycocyanin- and Spirulina extract-loaded gliadin fibers for active food packaging. *Food Chemistry: X, 22*, Article 101275. doi: 10/g8p446.
Guo, W., Zhu, S., Feng, G., Wu, L., Feng, Y., Guo, T., Yang, Y., Wu, H., & Zeng, M. (2020). Microalgae aqueous extracts exert intestinal protective effects in Caco-2 cells and dextran sodium sulphate-induced mouse colitis. *Food & Function, 11*(1), 1098–1109. https://doi.org/10.1039/C9FO01028A
Jiang, L., & Zheng, K. (2023). Xanthoceras sorbifolium Bunge leaf extract activated chia seeds mucilage/chitosan composite film: Structure, performance, bioactivity, and molecular dynamics perspectives. *Food Hydrocolloids, 144*, Article 109050. doi: 10/gsf26c.
Li, Q., Li, P., & Abbaspourrad, A. (2024). Using urea-shifting to create a natural blue, antioxidant emulsifier from phycocyanin. *Food Hydrocolloids, 155*, Article 110203. doi: 10/g8pvfr.
Li, Y., Zhang, Z., & Abbaspourrad, A. (2021). Improved thermal stability of phycocyanin under acidic conditions by forming soluble complexes with polysaccharides. *Food Hydrocolloids, 119*, Article 106852. doi: 10/gr86qr.
Li, Z., Yuan, B., Dashnyam, B., Cao, Y., Shan, H., Xu, X., Tan, M., Wang, Z., & Cao, C. (2023). Carboxylated chitosan improved the stability of phycocyanin under acidified conditions. *International Journal of Biological Macromolecules., 233*, Article 123474. doi: 10/gsdqr6.
Liu, J., Cheng, D., Zhang, D., Han, L., Gan, Y., Zhang, T., & Yu, Y. (2022). Incorporating ε-Polylysine hydrochloride, tea polyphenols, Nisin, and ascorbic acid into edible coating solutions: Effect on quality and shelf life of marinated eggs. *Food and Bioprocess Technology, 15*(12), 2683–2696. doi: 10/gqwdt3.
Liu, L., Jin, R., Hao, J., Zeng, J., Yin, D., Yi, Y., … Li, B. (2020). Consumption of the fish oil high-fat diet uncouples obesity and mammary tumor growth through induction of reactive oxygen species in Protumor macrophages. *Cancer Research, 80*(12), 2564–2574. doi: 10/gh26j9.
Liu, X., Liao, W., & Xia, W. (2023). Recent advances in chitosan based bioactive materials for food preservation. *Food Hydrocolloids, 140*, Article 108612. doi: 10/gr5cq6.
Min, Y., Dong, S., Su, M., Zhao, Y., & Zeng, M. (2020). Physicochemical, microbiological and sensory quality changes of tissues from Pacific oyster (*Crassostrea gigas*) during chilled storage. *Journal of Food Science and Technology, 57*(7), 2452–2460. doi: 10/gnqzsg.
Münch, K., Takeuchi, M., Tuinier, R., Stoyanov, S., Schroën, K., Friedrich, H., & Berton-Carabin, C. (2024). Mixed interfaces comprising pea proteins and phosphatidylcholine: A route to modulate lipid oxidation in emulsions? *Food Hydrocolloids, 153*, Article 109962. doi: 10/g86qjw.
Omar, A. E., Al-Khalaifah, H. S., Osman, A., Gouda, A., Shalaby, S. I., Roushdy, E. M., … Amer, S. A. (2022). Modulating the growth, antioxidant activity, and Immunoexpression of Proinflammatory cytokines and apoptotic proteins in broiler chickens by adding dietary Spirulina platensis Phycocyanin. *Antioxidants, 11*(5), 991. doi: 10/g8ps9t.
Radomirovic, M., Minic, S., Stanic-Vucinic, D., Nikolic, M., Van Haute, S., Rajkovic, A., & Cirkovic Velickovic, T. (2022). Phycocyanobilin-modified β-lactoglobulin exhibits increased antioxidant properties and stability to digestion and heating. *Food Hydrocolloids, 123*, Article 107169. doi: 10/gnc4x8.
Ran, R., Wang, L., Su, Y., He, S., He, B., Li, C., Wang, C., Liu, Y., & Chen, S. (2021). Preparation of pH-indicator films based on soy protein isolate/bromothymol blue and methyl red for monitoring fresh-cut apple freshness. *Journal of Food Science, 86*(10), 4594–4610. https://doi.org/10.1111/1750-3841.15884
Rathnasamy, S. K., Rajendran, D. S., Balaraman, H. B., & Viswanathan, G. (2019). Functional deep eutectic solvent-based chaotic extraction of phycobiliprotein using microwave-assisted liquid-liquid micro-extraction from Spirulina (Arthrospira platensis) and its biological activity determination. *Algal Research, 44*, Article 101709. doi: 10/g8p43j.
Shaikh, S., Yaqoob, M., & Aggarwal, P. (2021). An overview of biodegradable packaging in food industry. *Current Research in Food Science, 4*, 503–520. doi: 10/grb5h7.
Siddiqui, S. A., Singh, S., Bahmid, N. A., & Sasidharan, A. (2024). Applying innovative technological interventions in the preservation and packaging of fresh seafood products to minimize spoilage—A systematic review and meta-analysis. *Heliyon, 10*(8), Article e29066. doi: 10/g8qq8s.
Sun, J., Wei, Z., & Xue, C. (2023). Preparation and characterization of multifunctional films based on pectin and carboxymethyl chitosan: Forming microchambers for high-moisture fruit preservation. *Food Packaging and Shelf Life, 37*, Article 101073. doi: 10/gttvvr.
Tavakoli, S., Mubango, E., Tian, L., Bohoussou Ńdri, Y., Tan, Y., Hong, H., & Luo, Y. (2023). Novel intelligent films containing anthocyanin and phycocyanin for nondestructively tracing fish spoilage. *Food Chemistry, 402*, Article 134203. doi: 10/grq6s3.
Ul-Islam, M., Alabbosh, K. F., Manan, S., Khan, S., Ahmad, F., & Ullah, M. W. (2024). Chitosan-based nanostructured biomaterials: Synthesis, properties, and biomedical applications. *Advanced Industrial and Engineering Polymer Research, 7*(1), 79–99. doi: 10/g9bqrs.
Wang, H., Ouyang, Z., Hu, L., Cheng, Y., Zhu, J., Ma, L., & Zhang, Y. (2022). Self-assembly of gelatin and phycocyanin for stabilizing thixotropic emulsions and its effect on 3D printing. *Food Chemistry, 397*, Article 133725. doi: 10/gq5zqs.
Wang, K., Wang, H., Wu, Y., Yi, C., Lv, Y., Luo, H., & Yang, T. (2023). The antibacterial mechanism of compound preservatives combined with low voltage electric fields on the preservation of steamed mussels (*Mytilus edulis*) stored at ice-temperature. *Frontiers in Nutrition, 10*, 1126456. doi: 10/g8xpkc.
Yan, J., Zhang, Z., Lai, B., Wang, C., & Wu, H. (2024). Recent advances in marine-derived protein/polysaccharide hydrogels: Classification, fabrication, characterization, mechanism and food applications. *Trends in Food Science & Technology., 151*, Article 104637. doi: 10/g6n349.
Yin, H., Yuanrong, Z., Li, Y., Zijing, X., Yongli, J., Yun, D., Danfeng, W., & Yu, Z. (2022). Optimization of antibacterial and physical properties of chitosan/citronella oil film by electrostatic spraying and evaluation of its preservation effectiveness on salmon fillets. *Food Packaging and Shelf Life, 33*, Article 100891. doi: 10/gsv8j4.
Zhang, M., Yang, B., Yuan, Z., Sheng, Q., Jin, C., Qi, J., Yu, M., Liu, Y., & Xiong, G. (2023). Preparation and performance testing of corn starch/ pullulan /gallic acid multicomponent composite films for active food packaging. *Food Chemistry: X, 100782*. doi: 10/gsf2j8.
Zhang, Y., Han, Y., & Zhou, Z. (2024). A novel multifunctional composite film of oxidized dextran crosslinked chitosan and ε-polylysine incorporating protocatechuic acid and its application in meat packaging. *Food Hydrocolloids, 146*, Article 109186. doi: 10/gsqjmz.
Zhang, Z., Su, W., Li, Y., Zhang, S., Liang, H., Ji, C., & Lin, X. (2023). High-speed electrospinning of phycocyanin and probiotics complex nanofibrous with higher probiotic activity and antioxidation. *Food Research International, 167*, Article 112715. doi: 10/g8pvtk.
Zhao, M., Liu, Z., Zhao, Y., Gao, C., Wang, J., Xia, G., Li, C., & Zhou, D. (2024). Dielectric barrier discharge cold plasma collaborated with coconut exocarp flavonoids: A promising technology for oyster preservation under refrigerated storage. *LWT, 196*, Article 115888. doi: 10/gtq5df.